



HAL
open science

Femtosecond laser polishing of additively manufactured parts at grazing incidence

Nan Li, Peixun Fan, Qiuchi Zhu, Bai Cui, Jean-François Silvain, Yongfeng Lu

► **To cite this version:**

Nan Li, Peixun Fan, Qiuchi Zhu, Bai Cui, Jean-François Silvain, et al.. Femtosecond laser polishing of additively manufactured parts at grazing incidence. *Applied Surface Science*, 2023, 612, 155833 (10 p.). 10.1016/j.apsusc.2022.155833 . hal-03646753v2

HAL Id: hal-03646753

<https://hal.science/hal-03646753v2>

Submitted on 17 Jan 2023

HAL is a multi-disciplinary open access archive for the deposit and dissemination of scientific research documents, whether they are published or not. The documents may come from teaching and research institutions in France or abroad, or from public or private research centers.

L'archive ouverte pluridisciplinaire **HAL**, est destinée au dépôt et à la diffusion de documents scientifiques de niveau recherche, publiés ou non, émanant des établissements d'enseignement et de recherche français ou étrangers, des laboratoires publics ou privés.

Femtosecond laser polishing of additively manufactured parts at grazing incidence

Nan Li^{1,#}, Peixun Fan^{1,#,*}, Qiuchi Zhu¹, Bai Cui², Jean-Francois Silvain³ and Yong Feng Lu^{1,*}

¹*Department of Electrical and Computer Engineering, University of Nebraska, Lincoln, NE 68588, USA.*

²*Department of Mechanical and Materials Engineering, University of Nebraska, Lincoln, NE 68588, USA.*

³*CNRS, University of Bordeaux; Bordeaux I.N.P., ICMCB, UMR 5026, F-33608 Pessac, France.*

#Nan Li and Peixun Fan contributed equally to this work.

E-mails: ylu2@unl.edu and fanpeixun@gmail.com

Abstract

Surface polishing is usually a requisite for making additively manufactured (AM) parts ready for practical applications. Due to its advantages of being flexible and noncontact, laser polishing has attracted increasing research interest. In this research, femtosecond (fs) laser polishing was established to post-process both the top surfaces and sidewalls of AM parts. The challenge to remove three levels of roughness (i.e., the initial surface roughness of the AM parts, the undulations newly introduced during fs laser polishing, and the micro-nanoscale surface features induced by fs laser irradiation) was identified and addressed. Mirror surfaces with $S_a < 200$ nm were achieved on stainless steel parts printed with an initial roughness > 20 μm . Both parallel- and perpendicular-incidence were investigated for the polishing, with the former verified to be more effective in eliminating the initial roughness of the AM parts, due to the elongated focal intensity profile of a Gaussian beam irradiated on the AM part surfaces. The challenge of forming three-zone surfaces during the parallel-incidence was further addressed through a grazing-incidence

polishing approach, and uniform smooth surfaces were realized. Fine-tuning the laser power enabled controlling the submicron surface features formed under fs laser irradiation, which determined the final achievable surface roughness.

Keywords: Additive manufacturing, Femtosecond laser, Laser polishing, Grazing incidence

1. Introduction

Nowadays, additive manufacturing (AM) has been increasingly applied in various fields including automobile, aerospace, biomedicine, *etc.*, providing high flexibility in producing complex parts with desired performances [1-7]. Post-AM processing, polishing in particular, is usually necessary for improving the surface qualities of AM parts due to their intrinsic rough surfaces (typically $Ra > 15 \mu\text{m}$) resulting from the line-by-line and layer-by-layer printing process and the insufficient melting of the printing powders on surfaces [8,9]. Among different polishing techniques, laser polishing has attracted increasing research interest for achieving high-quality surface finishes due to its advantages of being flexible, noncontact, and less material dependence.

Laser polishing primarily uses continuous-wave (CW) or long-pulse [above nanosecond (ns)] lasers to melt thin surface layers, which promotes the re-flow or re-distribution of surface materials to reduce surface roughness [10,11]. For AM parts, surface polishing of titanium alloy [12-15], nickel alloy [15], and stainless steel [16-18] has been realized using ns and CW lasers. However, laser polishing through thermal melting is usually dependent on the initial surface roughness of AM parts. Surfaces with low initial roughness (e.g., 1-8 μm) can be smoothed down to nanoscale roughness [12,16,19,20], whereas surfaces with high initial roughness (e.g., 8-25 μm) can hardly be smoothed to roughness below 2 μm [21-24]. In addition, critical applications (e.g., optical, electrical, and biomedical devices) usually have strict requirements on surface microstructures,

compositions, and properties, ruling out the thermal-melting based methods which may cause surface microstructural and compositional changes or induce residual stresses and surface distortions [25]. It is also challenging to polish materials sensitive to heat or with high melting points using thermal melting processes [26-31].

In the past decade, femtosecond (fs) lasers have been recognized as a powerful tool for precision machining and micro/nanofabrication [32-35] due to their advantages over CW and long-pulse lasers, including having less thermal effect and minimal influence on the initial surface compositions. Different from the CW and long-pulse laser polishing, which is mainly an equal-material manufacturing process, fs laser processing mainly utilizes a subtractive ablation process that can not only reduce the surface roughness but also provides a second chance to improve the dimensional accuracies of three-dimensional (3D) parts. The fs laser polishing could be used either as an alternative to or in combination with CW and long-pulse laser polishing to achieve the lowest surface roughness in a more efficient manner. Due to its promising potential, a few attempts have been made in using fs laser ablation to polish planar surfaces, mainly with initially low roughness [36-38]. Nevertheless, fs laser polishing of 3D AM parts is yet to be fully explored.

In this study, fs laser polishing was established to post-process both the top surfaces and sidewalls of AM parts. The advantage of parallel-incidence over perpendicular-incidence polishing in realizing lower roughness was identified and ascribed to different laser-matter interactions occurring at different angles of incidence (AOI). Further, to address the challenge of forming three-zone surfaces during parallel incidence (AOI = 90°), a grazing-incidence (i.e., with grazing angles (GA) of 1-5°) was used, which improved the surface finish of the AM parts over 100 times. Surface roughness down to < 200 nm was uniformly achieved on the surfaces with initial roughness > 20 μm (Fig. 1). The evolution of submicron surface features under fs laser polishing were also

investigated. Lower surface roughness was achieved when the dominating surface features changed from continuous ripples to random, finer particles. This research has laid a foundation to make fs laser polishing an effective technique for post-processing AM parts.

2. Materials and methods

As a widely used engineering material, SAE 316L stainless steel was selected as a typical example in this research. The specimens were selectively laser-melted blocks of $10 \times 10 \times 3 \text{ mm}^3$ with an initial surface roughness of $Sa = 15\text{-}28 \text{ }\mu\text{m}$, which were obtained from Proto Labs, Inc. The laser polishing was conducted in open atmosphere using a Tangor laser system which works at a wavelength of 1030 nm and tunable pulse durations of 400 fs – 10 ps (Amplitude Laser, Inc.). The *p*-polarized laser beam was scanned by a galvanometer scanner (SCANLAB GmbH) and focused to a spot of about 30 μm in diameter by an F-theta lens with a focal length of 70 mm. The scanning field of the galvanometer scanner is $\sim 30 \times 30 \text{ mm}^2$. The AOI was controlled by a GN1 goniometer (Thorlabs) which is a device capable of rotating or tilting an object precisely, within a small angular range. The specimens together with the goniometer were fixed on an X-Y-Z stage which can reach travel ranges of $300 \times 300 \times 50 \text{ mm}^3$. The blocks of $10 \times 10 \times 3 \text{ mm}^3$ in size were used only for demonstration of the fs laser polishing approach. Dimensions of AM parts that can be polished are determined by the scanner and stages used. Surface roughness and 3D morphology images were measured and collected using either a VK-X200K laser scanning microscope (LSM, Keyence) or a NewView 8000 3D optical surface profiler (Zygo). The microstructures on the polished surfaces were characterized using an FEI Helios Nanolab 660 dual-beam field-emission scanning electron microscope (SEM) which was equipped with an energy dispersive X-ray spectroscopy (EDS) detector. X-ray diffraction (XRD) analyses were performed on a Bruker-AXS D8 diffractometer.

A three-step polishing approach was developed (i.e., sequentially by coarse polishing, precision polishing, and finishing steps) for the parallel- and grazing-incidence polishing, as schematically shown in Fig. S1. In each step, the fs laser scanning was continuously performed via the galvanometer scanner while continuously lowering the focal plane through a Z-stage until the entire depth was polished. Subsequently, the focal plane was moved back to the top surface to conduct the next step. The specific processing parameters for each step were listed in Table 1. Herein, scanning times refer to the number of laser scans that were evenly made within every 1 mm-depth range. The processing parameters in Table 1 were optimized in our preliminary experiments. The main difference between the coarse and precision polishing steps was that higher pulse energies were used in the coarse polishing to produce a relatively flat base for the subsequent precision polishing, while a higher pulse repetition rate was used in the precision polishing to realize a more uniform surface. Surface material layers of 60 and 20 μm thicknesses were removed through the coarse and precision polishing steps, respectively. The final finishing step was used to further modify and smooth the surfaces from the precision polishing step, without feeding the fs laser to remove more surface materials. Although few deep cavities may not be completely removed, most surface areas of the AM specimens used in this research can be smoothed by removing 80 μm surface layers. For AM parts having rougher initial surfaces, the complete removal of all surface defects can be realized by simply increasing the thickness of surface layers to be removed in the coarse polishing step. Such a three-step approach can be used to realize both lower surface roughness and higher processing efficiency.

3. Results and discussion

3.1 Top surface and sidewall polishing of three-level roughness

The initial top surfaces and sidewalls of the as-printed samples via selective laser melting were

obviously rough and occupied by incompletely melted printing powders, laser printing tracks, and random surface defects (e.g., cracks and voids) (Fig. 1a). Bumps were also observed at the edges between the top surface and sidewalls (Fig. 1b). After fs laser polishing, both the top surface and sidewalls were remarkably smoothed. The edges between the top surface and sidewalls were also sharpened (Fig. 1d,e). The polished surfaces became mirror-like surfaces that can show reflections of objects (e.g., a tweezer) near them (Fig. 1d), indicating the effectiveness of the fs laser as a tool for reducing surface roughness.

Table 1. Summary of the process parameters in fs laser polishing

Specific parameters	Coarse polishing	Precision polishing	Finishing
Laser power	Optimized in Figs. 5, 6	Optimized in Fig. 7	Optimized in Fig. S6
Pulse duration (fs)	400	400	400 fs - 10 ps
Repetition rate (kHz)	66	99	99
Scanning speed (m/s)	1	1	1
Scanning times per mm	1000	1000	1000

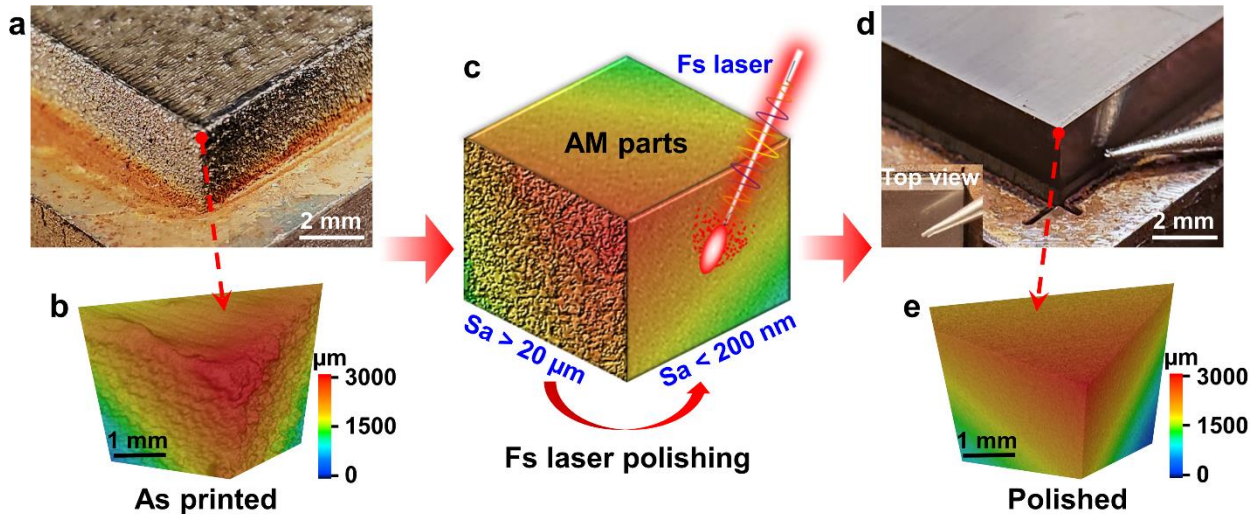


Fig. 1. Fs laser polishing and the representative results: (a) photo and (b) LSM image of the as printed part; (c) schematic of the fs laser polishing approach; (d) photo and (e) LSM image of the fs laser polished part; a tweezer was positioned near the polished sidewall (d) and the top surface (inset in (d)) to show the mirror-like surfaces achieved.

Specifically, three levels of roughness need to be removed to achieve mirror-like surfaces: (i) the initial surface roughness of selective laser melted parts (Fig. 2a), including the laser printing tracks and incompletely melted powders, *etc.*, (ii) the undulations introduced by fs laser scanning during the polishing process, and (iii) the micro-nanoscale surface features induced by fs laser irradiation. Therefore, the key to fs laser polishing AM parts is to minimize the initial roughness while preventing the formation of new undulations and micro-nanoscale features. Two different ways in which the fs laser was incident on the AM parts were investigated, i.e., the perpendicular incidence (AOI = 0°, or top-surface polishing, Fig. 2b) and the parallel incidence (AOI = 90°, or sidewall polishing, Fig. 2e). Various conditions were investigated for the perpendicular-incidence polishing (Figs. S2 and S3). However, it was found that the fs laser polishing at perpendicular incidence could not sufficiently reduce the initial roughness (Figs. 2c,d). For example, shallower laser printing tracks and deep cavities can still be observed on the surfaces, covered with some micro-nanoscale features generated by fs laser irradiation (Figs. 2d and S3). In contrast, the fs laser polishing at the parallel incidence can eliminate the initial roughness, leaving only slight undulations from fs laser scanning and micro-nanoscale features induced by fs laser irradiation (Figs. 2f,g).

The advantage of the parallel-incidence over perpendicular-incidence polishing is ascribed to the elongated focal intensity profile of a Gaussian beam. Usually, the depth of focus (F_d , defined as twice of the Rayleigh length) of a Gaussian laser beam is much larger than its beam waist. The depth of focus is determined by the laser wavelength (λ) and beam waist radius (w_0) as,

$$F_d = \frac{2\pi w_0^2}{\lambda}. \quad (1)$$

Calculated from Eq. (1), the depth of focus of the fs laser used in this research was 1372 μm , which was over 45 times of the beam waist (i.e., 30 μm used in this study). As a result, thin material

layers were simultaneously removed from both the peak and valley areas at perpendicular incidence, creating new peaks and valleys (Fig. S4b). Therefore, the laser printing tracks from the selective laser melting process could be reduced but not be sufficiently removed. At parallel incidence, the materials at different heights were not simultaneously ablated but successively removed due to the small beam waist. Therefore, the peak areas were preferentially ablated layer by layer (Fig. S4c), which significantly reduced the initial surface roughness of AM parts.

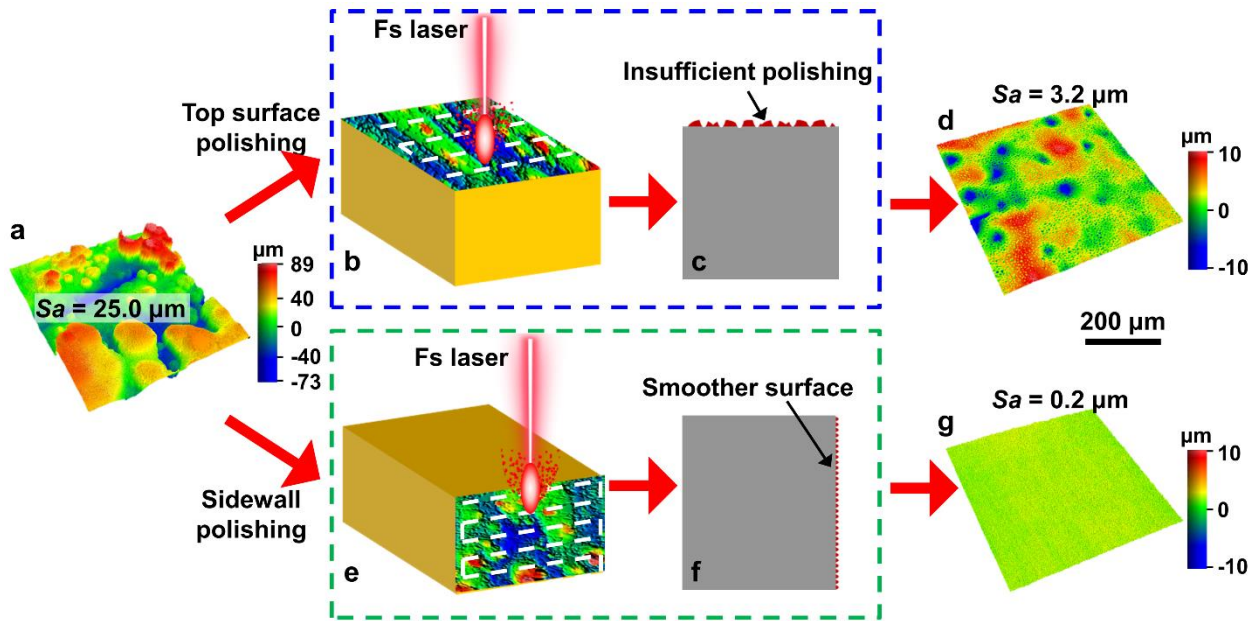


Fig. 2. Comparison of the fs laser perpendicular- and parallel-incidence polishing: (a) a typical Zygo image of the as-printed surfaces; (b), (c), and (d) schematic of process, schematic of effect, and a typical Zygo image for the perpendicular-incidence polishing, respectively (processing parameters: laser power = 1 W, repetition rate = 99 kHz, scanning speed = 1 m/s, hatching distance = 5 μm , scanning times = 800); (e), (f), and (g) schematic of process, schematic of effect, and a typical Zygo image for the parallel-incidence polishing, respectively (using the parameters in Table 1 with a laser power of 9.4, 11, and 11 W for the coarse polishing, precision polishing, and finishing steps, respectively).

3.2 Grazing-incidence fs laser polishing

Despite its advantages in achieving smoother surfaces, the fs laser polishing at parallel

incidence ($\text{AOI} = 90^\circ$) encountered a challenge of forming three-zone surfaces in the experiments. Three zones were observed on the fs laser polished areas: the top rough zone, the middle smooth zone, and the bottom rough zone (Fig. 3a,b). The as-printed zone to be polished was below the bottom rough zone. Both the top and bottom rough zones resulted from fs laser ablation under out-of-focus conditions (Fig. 3b). The top zone was initially smoothed when the fs laser was focused there. As the fs laser polishing went deeper with the top zone being re-ablated under out-of-focus conditions, the top zone became rough again. The bottom zone was always ablated by the fs laser under out-of-focus conditions and, hence, was insufficiently polished.

As evidenced in Fig. 3c, focusing the fs laser on the top of the sidewall (e.g., depth (Z) = 0.25 mm) initially produced a narrow smooth zone there (the smooth zone) and a wide rough zone below (i.e., the bottom rough zone). As the fs laser polishing went deeper (e.g., $Z = 0.5$ mm), the bottom rough zone also moved down, and the smooth zone was widened. However, when the fs laser polishing went further deeper (e.g., $Z = 0.7$ mm), it damaged the top part of the smooth zone and formed a top rough zone. As the fs laser polishing went even deeper (e.g., $Z = 1$ mm), the top rough zone was widened to ~ 260 μm . Two clear boundaries between the three zones can be observed, indicating the evolution of these three zones. Since the bottom rough zone can be eventually smoothed as the fs laser polishing continuously goes deeper, the key challenge of overcoming the three-zone surfaces and obtaining uniform smooth surfaces is to remove the top rough zone.

The formation of the top rough zone under out-of-focus conditions was caused by the divergence of the fs laser beam. In the experiment, the diameter (D) of the fs laser beam entering the galvanometer scanner was ~ 10 mm and the focal length (f) of the F-theta lens was 70 mm. Therefore, the half divergence angle can be estimated by

$$\theta = \arctan\left(\frac{D}{2f}\right), \quad (2)$$

which was $\sim 4.1^\circ$. To prevent the formation of the top rough zone, the AOI used for fs laser polishing needs to be adjusted accordingly.

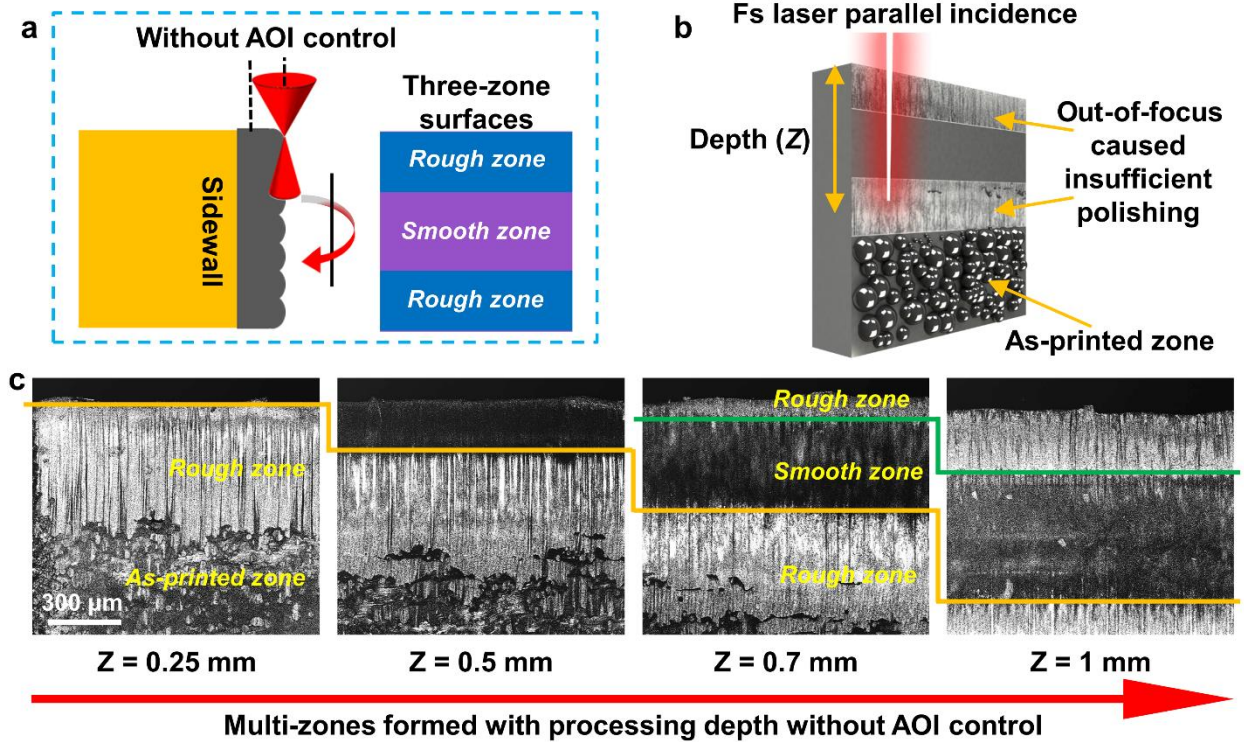


Fig. 3. The challenge of forming three-zone surfaces during fs laser polishing at parallel incidence: (a) schematics of the three-zone surfaces from both side (left) and front (right) views; (b) 3D schematic of the formation of the three-zone surfaces; (c) LSM images showing the evolution of the three-zone surfaces as the fs laser polishing went deeper. Only the coarse polishing step was applied here.

Since the divergence angle of the laser beam is small, only small GAs (e.g., $0-5^\circ$) were tested, through which a grazing-incidence fs laser polishing approach was developed (Fig. 4a,b). As shown in Fig. 4c, a wide top rough zone was formed at $GA = 0^\circ$. As larger GAs were used, the width of the top rough zone was gradually reduced until it was too small to measure (Fig. 4c,d). A GA above 4° successfully prevented the re-ablation of the top zone, which is consistent with the

half divergence angle estimated through Eq. (2). At the same time, the surface roughness stayed at low levels below $1\ \mu\text{m}$ (Fig. 4e), confirming the capability of the grazing-incidence fs laser polishing in achieving uniform and smooth surfaces. Both the smooth top surface and sidewalls of the AM part in Fig. 1d were achieved through the grazing-incidence fs laser polishing. The sidewalls were firstly polished one by one. Then, the AM part was flipped by 90° to have the initial top surface stand vertically where the grazing-incidence fs laser polishing was performed, as shown in Fig. S5.

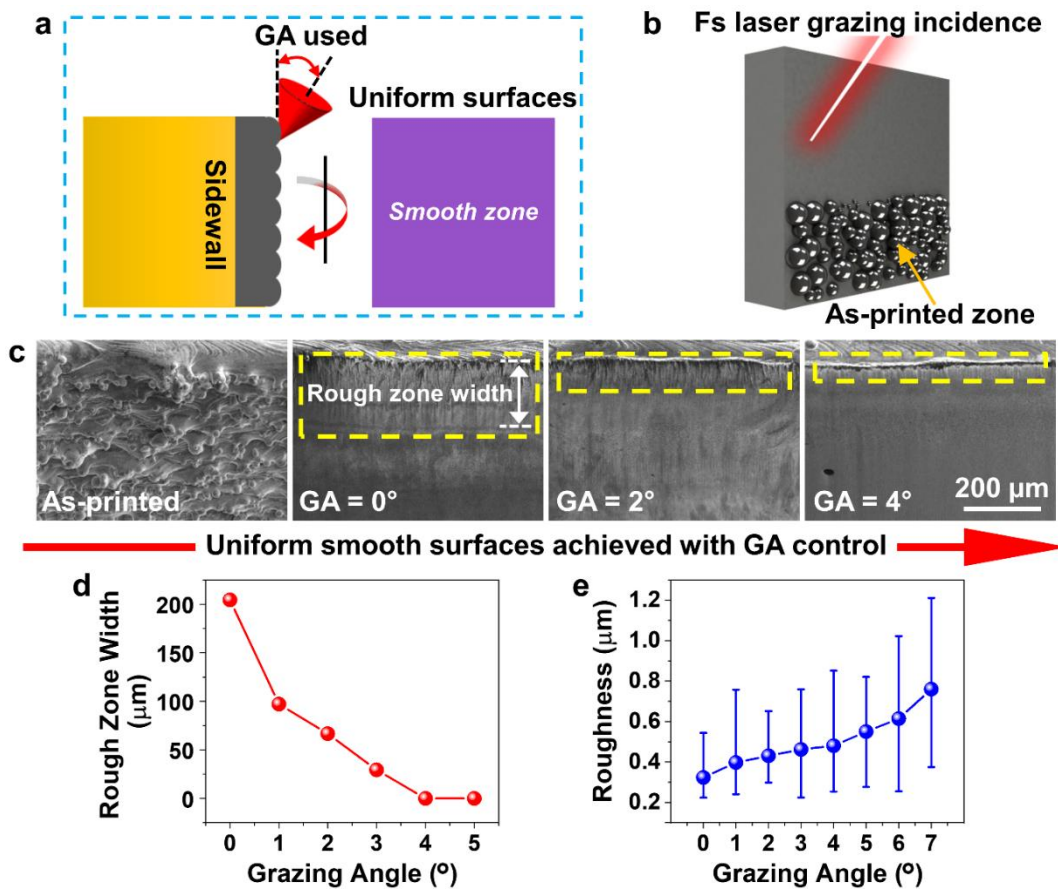


Fig. 4. Grazing-incidence fs laser polishing for achieving uniform smooth surfaces: (a) schematics of GA used from the side view (left) and the uniform surfaces from the front view (right); (b) 3D schematic of the grazing-incidence fs laser polishing; (c) SEM images showing the reduction of the top rough zone as larger GAs were used; evolution of the width of the top rough zone (d) and surface roughness (e) with the GA. Both the coarse and precision polishing steps were applied here.

3.3 Optimization of grazing-incidence fs laser polishing for minimizing surface roughness

A systematic investigation was performed to identify the evolution of the surface roughness of AM parts with the surface dominating features during the grazing-incidence fs laser polishing, clarifying how the surface roughness was gradually reduced in three levels by adjusting the fs laser polishing process. As shown in Fig. 5, the fs laser reduces the initial surface roughness primarily through a layer-by-layer ablation mechanism. As thicker material layers were removed, the surfaces became smoother.

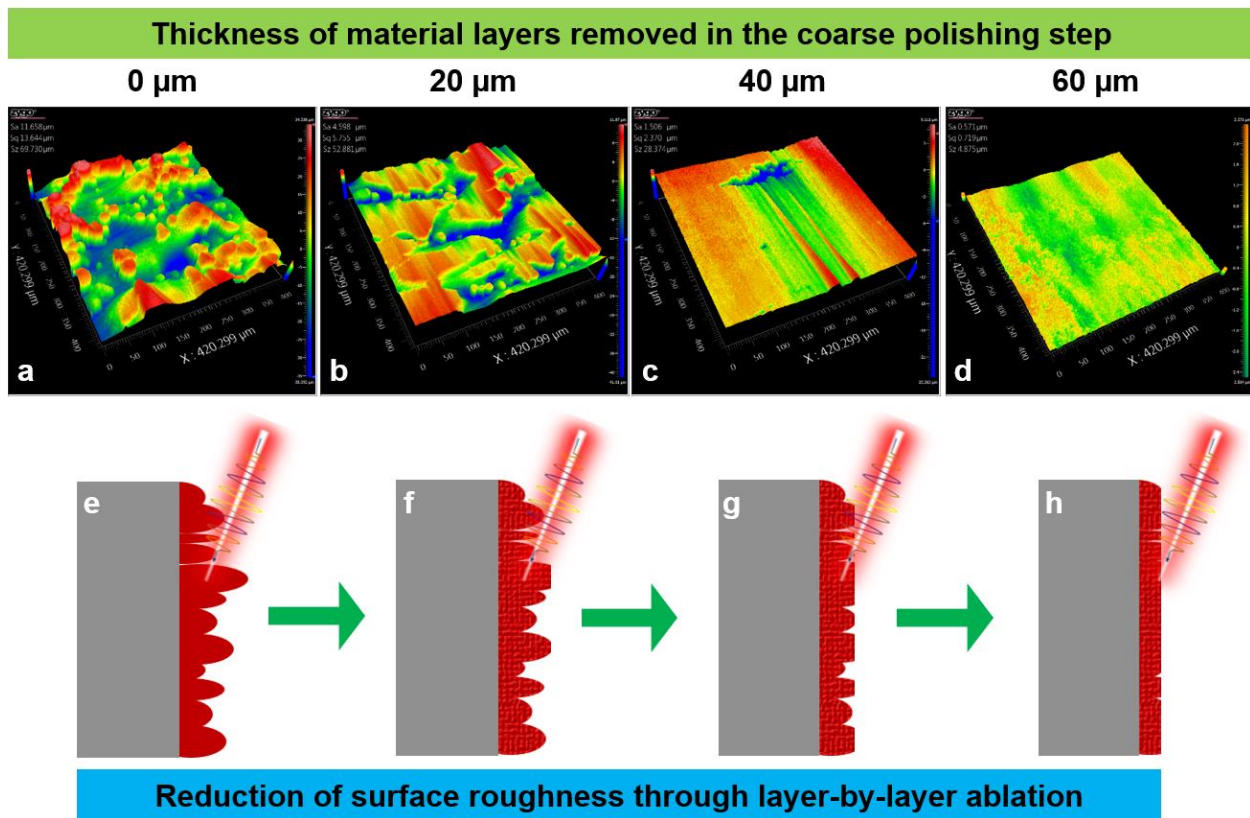


Fig. 5. Gradual reduction of initial surface roughness of AM parts in the fs-laser coarse polishing step: (a)-(d) typical Zygo images of the surfaces polished after material layers of different thickness were removed; (e)-(h) corresponding schematics of the fs laser polishing via a layer-by-layer ablation mechanism. Processing parameters used: laser power = 9.4 W, repetition rate = 66 kHz, scanning speed = 1 m/s, GA = 4°, scanning times = 1000.

Even when it was programmed to remove material layers of a same thickness (e.g., 60 μm), the obtained surface qualities varied with the specific processing parameters used. As an example, Fig. 6 shows the influences of the two main parameters (i.e., the laser power and the scanning time) on the surface roughness of the AM parts. Briefly, when higher laser power and more scanning times were applied, the initial roughness (Level (i)) including the laser printing tracks and incompletely melted powders became blurry, as indicated by the arrow from the bottom-left to the top-right corners in Fig. 6. Specifically,

- When less laser scans were applied within a unit depth range (e.g., scanning times = 250), the initial roughness from selective laser melting remained on the surfaces. As the laser power was increased from 7.9 to 11.0 W, the laser printing tracks and incompletely melted powders were reduced, and the surfaces became less bumpy.
- Using more laser scans within a unit depth range (e.g., scanning times = 500) significantly reduced the initial roughness at all laser powers between 7.9–11.0 W. Additionally, the laser printing tracks were flattened and the undulations introduced by the fs laser polishing (much finer than the laser printing tracks) were observed. At this stage, the undulations introduced by the fs laser scanning during the polishing process (Level (ii)) dominated the surfaces and accounted for the remaining surface roughness.
- When the number of laser scans applied within a unit depth range was further increased (e.g., scanning times = 1000), the undulations resulting from the fs laser polishing were reduced and even became unobservable. The dominating features on the surfaces of the AM parts became the submicron features induced by the fs laser (e.g., nanoripples and nanoparticles), achieving a surface roughness of the magnitude of ~ 100 nm.

The observations described above indicate that a careful control over the fs laser processing

conditions (i.e., to maximumly reduce the initial roughness while suppressing the undulations and submicron features generated by fs laser simultaneously) is necessary for an effective fs laser polishing.

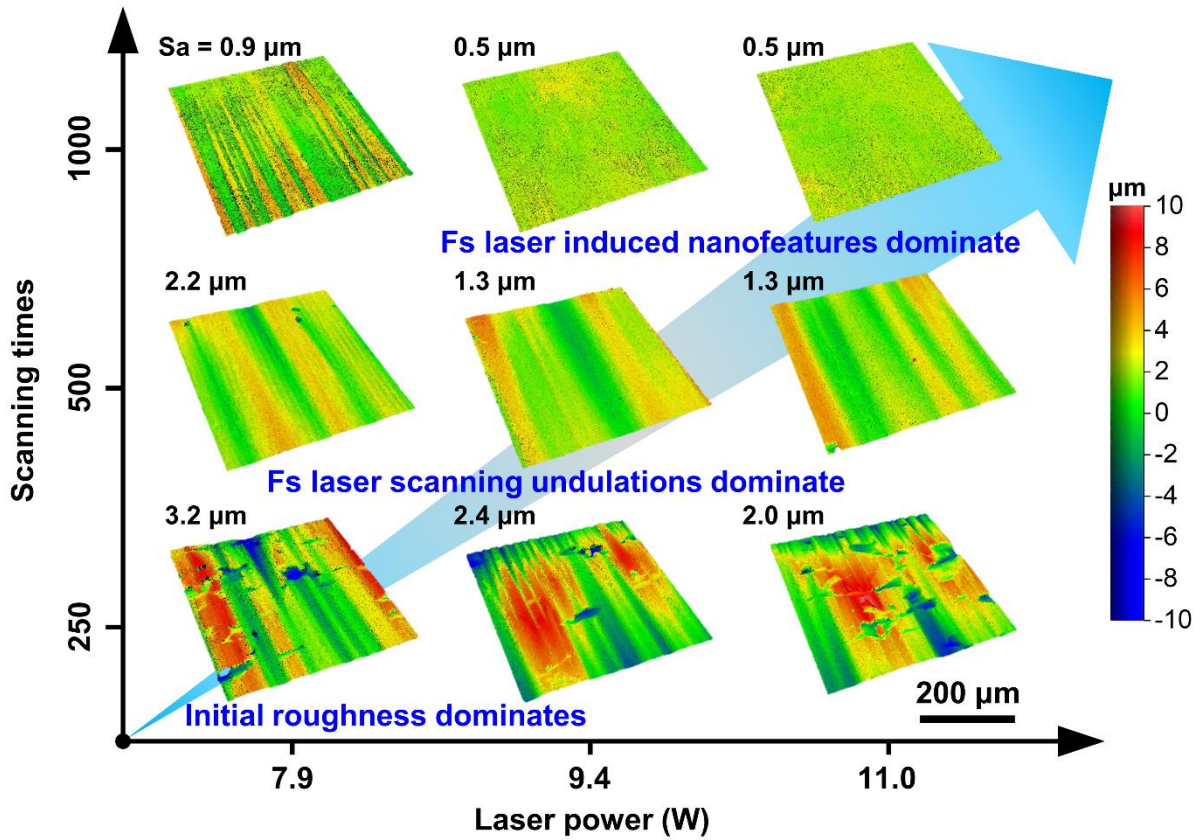


Fig. 6. A systematic investigation on the evolution of surface roughness with surface dominating features. Only the coarse polishing step was applied here.

The formation of submicron features on solid surfaces under fs laser irradiation has been extensively studied [39,40]. The dependence of the final achievable surface roughness on such submicron features distinguishes fs laser polishing from CW and long-pulse laser polishing. To investigate how fs-laser-induced submicron features evolve during the polishing process, rather than during the fs laser irradiation of smooth solid surfaces as in previous studies, the fs laser-polished surfaces were carefully examined through SEM.

Three types of submicron features were observed as the fs laser polishing conditions vary. Taking laser power as an example (Fig. 7a-c), the submicron features evolved from continuous ripples to discontinuous ripples (ripples together with particles) and then to finer particles as the laser power was increased from 4.6 to 7.3 and then to 11.0 W. As a result, the surface roughness was reduced from above 1 μm to only 400 nm. The discontinuity of the ripples (i.e., the transition from ripples to particles) at a higher laser power was caused by more intense laser ablation with slight local melting. Further increasing the laser power to 11.0 W not only turned most of the submicron features on the polished surfaces to particles, but also reduced the size of these particles, which minimized the surface roughness. Furthermore, a fast-Fourier-transformation (FFT) analysis was conducted on the SEM images. Bright spots can be observed in the FFT images at lower laser powers but became blurry at higher laser powers, confirming that the surface features evolved from more regular to more random ones, which are favorable for achieving lower surface roughness.

Specifically, the characteristics of submicron ripples can be defined by their vertical heights and horizontal periodicities (d). The formation of both low-spatial-frequency and high-spatial-frequency ripples on various solid surfaces under fs laser irradiation have been extensively studied [41]. In our experiments, the low-spatial-frequency ripples were found to dominate the surfaces. Previous studies have correlated the periodicities of low-spatial-frequency ripples induced by p -polarized fs laser to laser wavelengths and incident angles as [42],

$$d = \frac{\lambda}{1 \pm \sin(\text{AOI})}. \quad (3)$$

At a GA of 4° , the AOI is 86° . Hence, the periodicity of the fs-laser-induced ripples is 515.6 nm, as calculated from Eq. (3). As shown in Fig. 7a, the periodicity of the ripples formed during the grazing-incidence fs laser polishing is ~ 500 nm, which is consistent with the calculation. However,

few investigations have been made on the heights of the submicron ripples, although they can influence more on the surface roughness. As a simple estimation, the heights of the fs-laser-induced submicron ripples are usually of the same magnitudes as their periodicities, which also implies a range of surface roughness of 100-1000 nm.

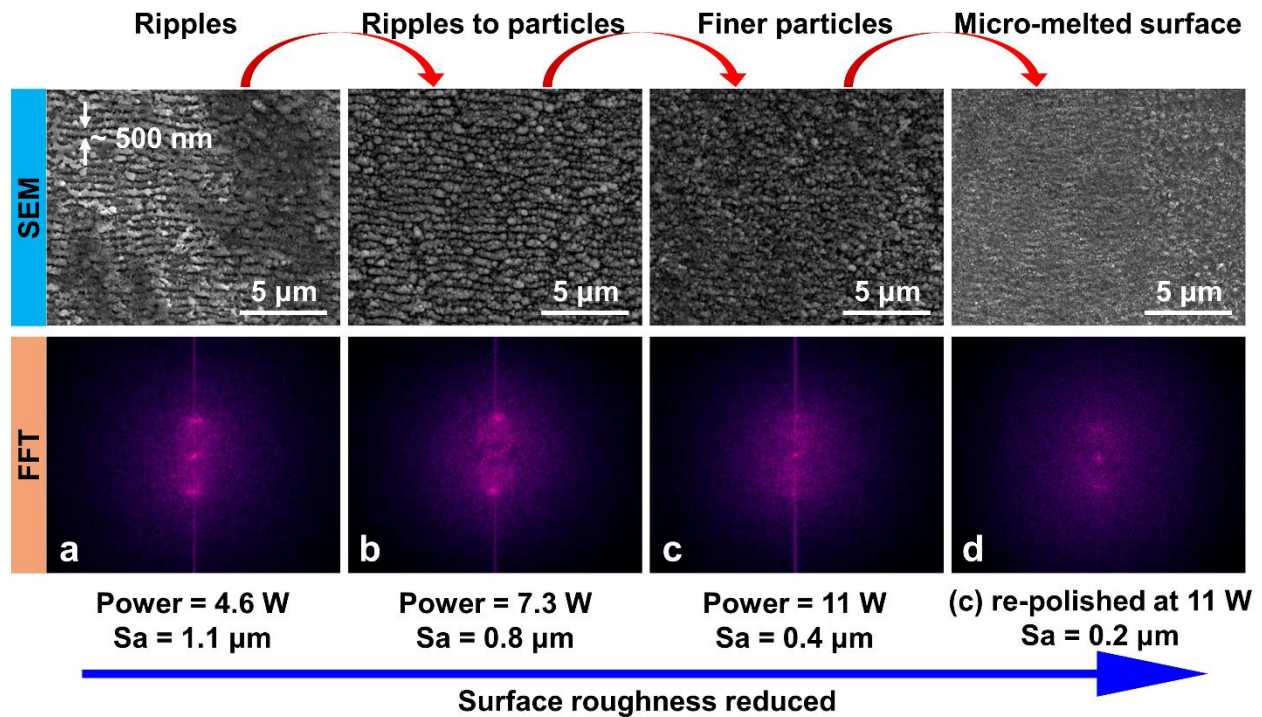


Fig. 7. Evolution of submicron surface features with different laser powers in fs laser polishing and their influence on the final surface roughness. (a-c) Both the coarse and precision polishing steps were applied. The power shown for (a-c) was used for the precision polishing, and the parameters for the coarse polishing were the same for (a-c). (d) The finishing step was conducted on (c).

To explore the potential to further smooth the fs-laser-induced submicron features and, hence, to reach lower surface roughness, a finishing step was conducted after completing both the coarse and precision polishing steps. Different pulse durations, pulse repetition rates, and laser powers were investigated for the finishing step (Fig. S6). Lower roughness values were achieved at the pulse duration of 400 fs compared with 1 and 10 ps. Surface roughness values even below 200 nm

were measured after the fs laser finishing step, where micro-melted surface regions were observed (Fig. 7d). Further investigations should focus on controlling and reducing the submicron features to achieve surface roughness below 100 nm using fs lasers. It is known that both the fs laser ablation/melting thresholds and the sizes of submicron features formed under fs laser irradiation vary among different materials. Therefore, we believe it is possible to realize even lower surface roughness on some other materials using the fs laser polishing approach established in this study. Besides, it was recently reported that continuous surface melting can even be realized by fs lasers (or ps lasers in more studies) through heat accumulation via MHz-level pulse repetition rates [43-46]. Such a fs-laser-induced continuous surface melting process could also benefit the achievement of extremely low surface roughness for AM parts.

3.4 Advantages of fs laser polishing

The surface compositions of the AM parts after the fs laser polishing were examined through XRD and EDS analyses. The three major peaks at 2θ of 43.55° , 50.55° , and 74.7° in the XRD patterns (Fig. 8a) correspond to the (111), (200), and (220) planes of the austenite (γ -Fe) phase, respectively. The positions of the three XRD peaks of the polished surface remained the same as the initial rough surface, indicating that no significant phase change occurred.

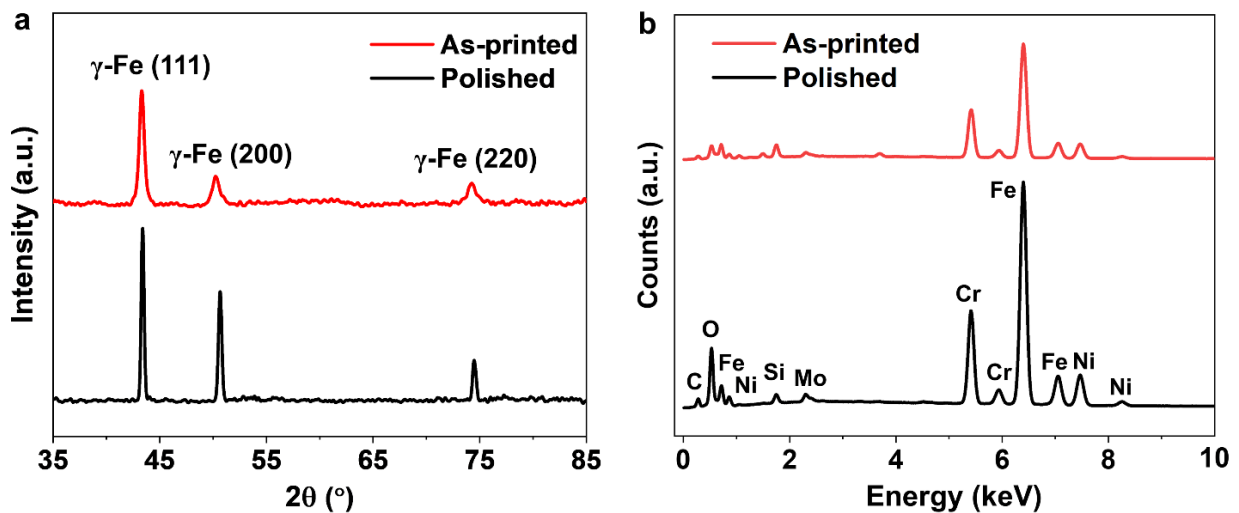


Fig. 8. (a) XRD and (b) EDS analyses on the polished and as-printed surfaces.

The EDS analyses further confirmed that the main element contents (Fe, Cr, Ni, Mo) were not obviously changed during the fs laser polishing (Fig. 8b and Table 2). The rise of the oxygen content indicates the occurrence of slight surface oxidation, which did not influence the main crystalline microstructures of the AM parts, according to the XRD results.

It is well-known that fs lasers can process almost any solids with little thermal effects. Therefore, chemical-composition and material-property changes usually seen in thermal treatments will be insignificant under fs laser irradiation. As for the influences of the fs-laser-induced submicron features on the surface physical-chemical properties, extensive understanding has been made through previous studies on various materials [33,34,47,48], which can also apply to the submicron features achieved after the three-step fs laser polishing.

Table 2. Chemical compositions of both the as-printed and polished surfaces determined by EDS.

Elements		Fe	Cr	Ni	Mo	C	O	Si
wt.%	As-printed	63.99	22.04	9.69	0.72	0.40	1.84	1.32
	Polished	62.61	21.34	10.31	0.64	0.53	4.34	0.22

As a comparison, representative results from previous studies on polishing AM parts with CW or long-pulse lasers were summarized in Fig. 9. It can be seen that the surface finish achieved through the fs laser polishing approach in this research is comparable to the best levels achieved by CW and long-pulse lasers. In addition, the effect of CW and long-pulse laser polishing shows an obvious dependence on the initial surface roughness. A final surface roughness of $Sa \sim 200$ nm was obtained through fs laser polishing the surface with an initial roughness of $Sa = 25 \mu\text{m}$, equivalent to $> 99\%$ improvement in the surface quality. It is also worth noting that although the experiments were implemented on 316L stainless steel in this research, the knowledge

accumulated and approaches developed in this study can be widely applied to polishing AM parts of other materials (e.g., metals, ceramics, polymers, and composites).

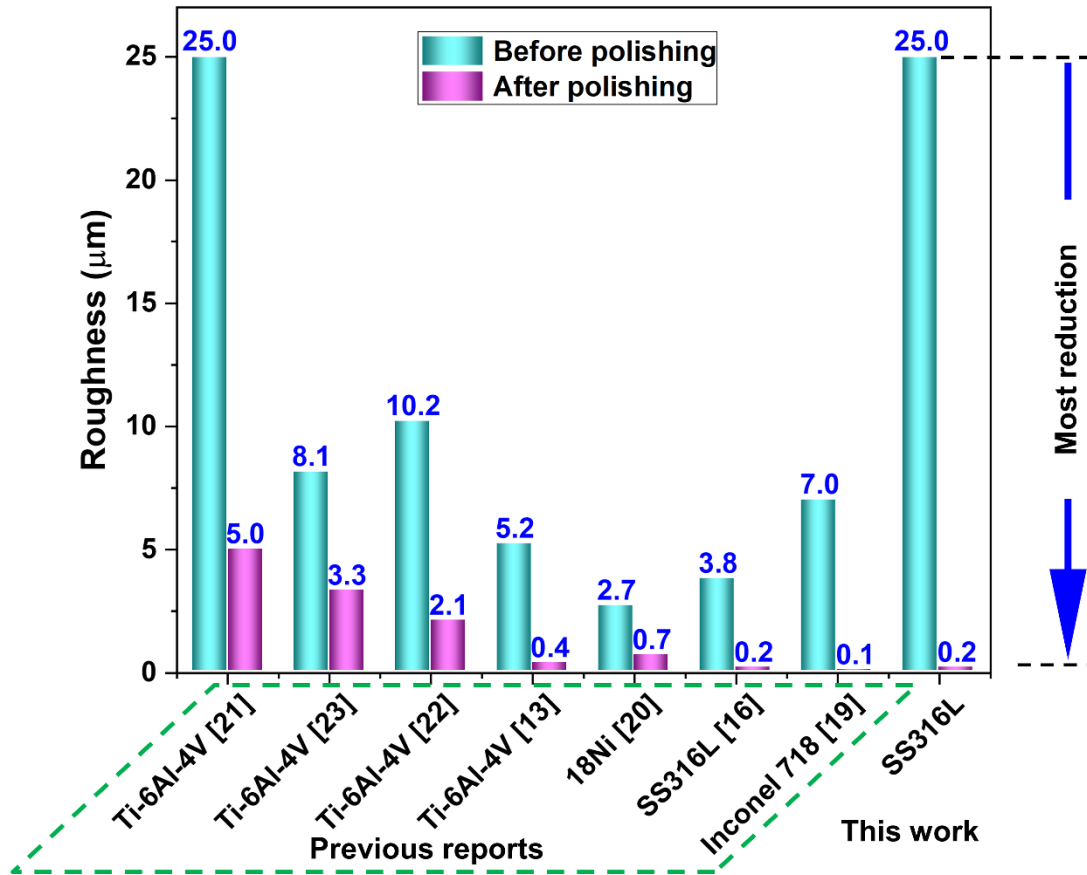


Fig. 9. Comparison of the roughness reduction between this work and previous reports.

Nevertheless, although it can be used to polish surfaces with high initial roughness, the fs laser polishing is not dedicated to this purpose. The results obtained in this research can support customizable polishing from different initial roughness levels towards different targeted ones, such as processes X1-Z1 shown in Fig. 10. Practical post-AM processing can comprise a series of approaches including the mechanical and/or chemical ones. Rather than replacing any existing post-AM processing approaches, the fs laser polishing can be used in combination with any of them. Regardless of the specific roughness levels to which the AM parts are processed by other

approaches, fs laser polishing can further improve the surface finishes.

Besides, the cuboid blocks were used only as an example of 3D AM parts, and the top surface and sidewalls of the cuboid blocks were also investigated as representative surfaces of 3D AM parts. The concepts and fundamentals established in this research can still apply when polishing AM parts with complex shapes. Specifically, hardware configurations and system integration with more flexible motion systems (e.g., translation stages with longer travel ranges, motorized rotation and tilt stages, multi-axis scanners and stages, *etc.*) may be needed to facilitate the continuous control over the fs laser scanning along non-flat surfaces to conduct the grazing-incident polishing.

From the point of view of practical applications, the efficiency of the fs laser polishing was also estimated, which is $\sim 30 \text{ min/cm}^2$, limited by the current parameter set and hardware system. Since the main concepts and fundamentals have been demonstrated in this research, the fs laser polishing approach can be flexibly extended to higher parameters (e.g., higher laser power, pulse repetition rate, and scanning speed) and upgraded hardware systems, which can significantly increase the processing efficiency.

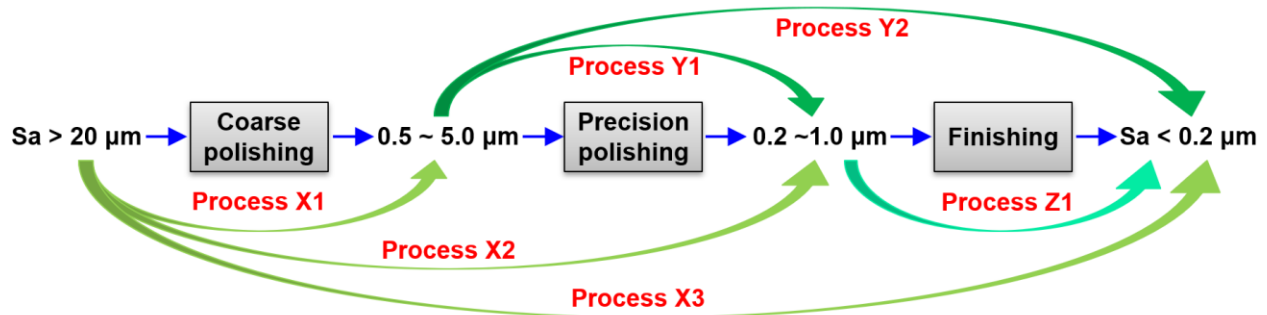


Fig. 10. Roadmap for customizable fs laser polishing approaches from different initial roughness levels towards different targeted ones.

4. Conclusions

In this study, fs laser polishing was established for post-processing both the top surfaces and

sidewalls of AM parts. The challenge of removing three levels of roughness was addressed, achieving mirror-like surfaces with a Sa < 200 nm on stainless steel parts with initial roughness > 20 μm, equivalent to > 99% improvement on the surface finish. Parallel-incidence polishing was found to be more effective than perpendicular-incidence polishing in eliminating the initial roughness of the AM parts, which was ascribed to the elongated focal intensity profile of the Gaussian beam. Furthermore, the grazing-incidence fs laser polishing approach was developed to solve the issue of forming three-zone surfaces during the parallel incidence and produce uniform, smooth surfaces. The submicron surface features formed under fs laser irradiation determined the final achievable surface roughness. Fine-tuning the laser power enabled controlling the submicron surface features, where random and finer particles were more favorable for reaching lower surface roughness than continuous ripples. No obvious composition changes were induced during fs laser polishing, and the original material properties were well preserved. This research demonstrates the capability of fs lasers in surface polishing and opens a new avenue for post-processing AM parts.

Acknowledgement

This study was supported by the National Science Foundation (CMMI 1826392) and the Nebraska Center for Energy Sciences Research (NCESR). The research was performed in part in the Nebraska Nanoscale Facility: National Nanotechnology Coordinated Infrastructure and the Nebraska Center for Materials and Nanoscience, which are supported by the National Science Foundation under Award ECCS: 1542182, and the Nebraska Research Initiative.

References

- [1] T.D. Ngo, A. Kashani, G. Imbalzano, K.T.Q. Nguyen, D. Hui, Additive manufacturing (3D printing): A review of materials, methods, applications and challenges, *Compos. B. Eng.* 143 (2018) 172-196. <https://doi.org/10.1016/j.compositesb.2018.02.012>

- [2] B. Blakey-Milner, P. Gradl, G. Snedden, M. Brooks, J. Pitot, E. Lopez, M. Leary, F. Berto, A. du Plessis, Metal additive manufacturing in aerospace: A review, *Mater. Des.* 209 (2021) 110008. <https://doi.org/10.1016/j.matdes.2021.110008>
- [3] Y. Wang, A. Ahmed, A. Azam, D. Bing, Z. Shan, Z. Zhang, M.K. Tariq, J. Sultana, R.T. Mushtaq, A. Mehboob, C. Xiaohu, M. Rehman, Applications of additive manufacturing (AM) in sustainable energy generation and battle against COVID-19 pandemic: The knowledge evolution of 3D printing, *J. Manuf. Syst.* 60 (2021) 709-733. <https://doi.org/10.1016/j.jmsy.2021.07.023>
- [4] L. Yin, J. Doyhamboure--Fouquet, X. Tian, D. Li, Design and characterization of radar absorbing structure based on gradient-refractive-index metamaterials, *Compos. B. Eng.* 132 (2018) 178-187. <https://doi.org/10.1016/j.compositesb.2017.09.003>
- [5] J.C. Najmon, S. Raeisi, A. Tovar, Review of additive manufacturing technologies and applications in the aerospace industry, *Additive Manufacturing for the Aerospace Industry*, Elsevier Inc., Amsterdam, 2019, pp. 7-31. <https://doi.org/10.1016/b978-0-12-814062-8.00002-9>
- [6] V.V. Popov, Jr., G. Muller-Kamskii, A. Kovalevsky, G. Dzhenzhera, E. Strokin, A. Kolomiets, J. Ramon, Design and 3D-printing of titanium bone implants: brief review of approach and clinical cases, *Biomed. Eng. Lett.* 8(4) (2018) 337-344. <https://doi.org/10.1007/s13534-018-0080-5>
- [7] A. Liu, G.H. Xue, M. Sun, H.F. Shao, C.Y. Ma, Q. Gao, Z.R. Gou, S.G. Yan, Y.M. Liu, Y. He, 3D Printing Surgical Implants at the clinic: A Experimental Study on Anterior Cruciate Ligament Reconstruction, *Sci. Rep.* 6 (2016) 21704. <https://doi.org/10.1038/srep21704>

- [8] U. Ali, R. Esmailizadeh, F. Ahmed, D. Sarker, W. Muhammad, A. Keshavarzkermani, Y. Mahmoodkhani, E. Marzbanrad, E. Toyserkani, Identification and characterization of spatter particles and their effect on surface roughness, density and mechanical response of 17-4 PH stainless steel laser powder-bed fusion parts, *Mater. Sci. Eng., A* 756 (2019) 98-107. <https://doi.org/10.1016/j.msea.2019.04.026>
- [9] C. Guo, S. Li, S. Shi, X. Li, X. Hu, Q. Zhu, R.M. Ward, Effect of processing parameters on surface roughness, porosity and cracking of as-built IN738LC parts fabricated by laser powder bed fusion, *J. Mater. Process. Technol.* 285 (2020) 116788. <https://doi.org/10.1016/j.jmatprotec.2020.116788>
- [10] W. Zhang, K. Wong, M. Morales, C. Molpeceres, C.B. Arnold, Implications of using two low-power continuous-wave lasers for polishing, *Int. J. Extreme Manuf.* 2(3) (2020) 035101. <https://doi.org/10.1088/2631-7990/ab94c6>
- [11] A. Temmler, D. Liu, J. Luo, R. Poprawe, Influence of pulse duration and pulse frequency on micro-roughness for laser micro polishing (L μ P) of stainless steel AISI 410, *Appl. Surf. Sci.* 510 (2020) 145272. <https://doi.org/10.1016/j.apsusc.2020.145272>
- [12] Y. Tian, W.S. Gora, A.P. Cabo, L.L. Parimi, D.P. Hand, S. Tammam-Williams, P.B. Prangnell, Material interactions in laser polishing powder bed additive manufactured Ti6Al4V components, *Addit. Manuf.* 20 (2018) 11-22. <https://doi.org/10.1016/j.addma.2017.12.010>
- [13] C.P. Ma, Y.C. Guan, W. Zhou, Laser polishing of additive manufactured Ti alloys, *Optics and Lasers in Engineering* 93 (2017) 171-177. <https://doi.org/10.1016/j.optlaseng.2017.02.005>

- [14] S. Marimuthu, A. Triantaphyllou, M. Antar, D. Wimpenny, H. Morton, M. Beard, Laser polishing of selective laser melted components, *Int. J. Mach. Tools Manuf.* 95 (2015) 97-104. <https://doi.org/10.1016/j.ijmachtools.2015.05.002>
- [15] Y. Guan, Y. Li, H. Wang, Laser polishing of additive-manufactured Ti alloys and Ni alloys, in: J. Pou, A. Riveiro, J.P. Davim, *Additive Manufacturing*, Elsevier 2021, pp. 343-368. <https://doi.org/10.1016/b978-0-12-818411-0.00002-1>
- [16] D. Bhaduri, P. Penchev, A. Batal, S. Dimov, S.L. Soo, S. Sten, U. Harrysson, Z. Zhang, H. Dong, Laser polishing of 3D printed mesoscale components, *Applied Surface Science* 405 (2017) 29-46. <https://doi.org/10.1016/j.apsusc.2017.01.211>
- [17] L. Chen, B. Richter, X. Zhang, X. Ren, F.E. Pfefferkorn, Modification of surface characteristics and electrochemical corrosion behavior of laser powder bed fused stainless-steel 316L after laser polishing, *Addit. Manuf.* 32 (2020) 101013. <https://doi.org/10.1016/j.addma.2019.101013>
- [18] A. Lamikiz, J.A. Sánchez, L.N. López de Lacalle, J.L. Arana, Laser polishing of parts built up by selective laser sintering, *Int. J. Mach. Tools Manuf.* 47(12-13) (2007) 2040-2050. <https://doi.org/10.1016/j.ijmachtools.2007.01.013>
- [19] F. Zhihao, L. Libin, C. Longfei, G. Yingchun, Laser polishing of additive manufactured superalloy, *Procedia CIRP* 71 (2018) 150-154. <https://doi.org/10.1016/j.procir.2018.05.088>
- [20] J. dos Santos Solheid, H. Jürgen Seifert, W. Pfleging, Laser surface modification and polishing of additive manufactured metallic parts, *Procedia CIRP* 74 (2018) 280-284. <https://doi.org/10.1016/j.procir.2018.08.111>
- [21] S. Genna, G. Rubino, Laser finishing of Ti6Al4V additive manufactured parts by electron beam melting, *Appl. Sci.* 10 (2019) 183. <https://doi.org/10.3390/app10010183>

- [22] C. Liang, Y. Hu, N. Liu, X. Zou, H. Wang, X. Zhang, Y. Fu, J. Hu, Laser polishing of Ti6Al4V fabricated by selective laser melting, *Metals* 10 (2020) 191. <https://doi.org/10.3390/met10020191>
- [23] D. Zhang, J. Yu, H. Li, X. Zhou, C. Song, C. Zhang, S. Shen, L. Liu, C. Dai, Investigation of laser polishing of four selective laser melting alloy samples, *Appl. Sci.* 10 (2020) 760. <https://doi.org/10.3390/app10030760>
- [24] K. Bobe, W.G. Gutu, M. Sankar, U. Dixit, Experimental study and empirical modelling of laser surface finishing of silicon carbide, *Int. J. Addit. Subtractive Mater. Manuf.* 1 (2017) 290. <https://doi.org/10.1504/IJASMM.2017.089922>
- [25] L. Zhao, J. Cheng, M. Chen, X. Yuan, W. Liao, Q. Liu, H. Yang, H. Wang, Formation mechanism of a smooth, defect-free surface of fused silica optics using rapid CO2 laser polishing, *Int. J. Extreme Manuf.* 1(3) (2019) 35001. <https://doi.org/10.1088/2631-7990/ab3033>
- [26] C.E. Zak, C. Zhou, H.M. John, J.J. Alan, B.C. William, A.S. Tobias, Additive manufacturing of polymer-derived ceramics, *Science* 351(6268) (2016) 58-62. <https://doi.org/10.1126/science.aad2688>
- [27] G. Zhang, D. Carloni, Y. Wu, 3D printing of transparent YAG ceramics using copolymer-assisted slurry, *Ceram. Int.* 46(10) (2020) 17130-17134. <https://doi.org/10.1016/j.ceramint.2020.03.247>
- [28] D. Carloni, G. Zhang, Y. Wu, Transparent alumina ceramics fabricated by 3D printing and vacuum sintering, *J. Eur. Ceram. Soc.* 41(1) (2021) 781-791. <https://doi.org/10.1016/j.jeurceramsoc.2020.07.051>

- [29] J.R.C. Dizon, A.H. Espera, Q. Chen, R.C. Advincula, Mechanical characterization of 3D-printed polymers, *Addit. Manuf.* 20 (2018) 44-67. <https://doi.org/10.1016/j.addma.2017.12.002>
- [30] G. Zhang, Y. Wu, Three-dimensional printing of transparent ceramics by lithography-based digital projection, *Addit. Manuf.* 47 (2021) 102271. <https://doi.org/10.1016/j.addma.2021.102271>
- [31] N. Li, D. Qiao, S. Zhao, Q. Lin, B. Zhang, F. Xie, 3D printing to innovate biopolymer materials for demanding applications: A review, *Mater. Today Chem.* 20 (2021) 100459. <https://doi.org/10.1016/j.mtchem.2021.100459>
- [32] Q. Zhu, P. Fan, N. Li, T. Carlson, B. Cui, J. F. Silvain, J. L. Hudgins, Y. F. Lu, Femtosecond-laser sharp shaping of millimeter-scale geometries with vertical sidewalls, *Int. J. Extrem. Manuf.* 3(4) (2021) 045001. <https://doi.org/10.1088/2631-7990/ac2961>
- [33] P. Fan, B. Bai, M. Zhong, H. Zhang, J. Long, J. Han, W. Wang, G. Jin, General strategy toward dual-scale-controlled metallic micro-nano hybrid structures with ultralow reflectance, *ACS Nano* 11(7) (2017) 7401-7408. <https://doi.org/10.1021/acs.nano.7b03673>
- [34] Y. Zhang, Y. Jiao, C. Li, C. Chen, J. Li, Y. Hu, D. Wu, J. Chu, Bioinspired micro/nanostructured surfaces prepared by femtosecond laser direct writing for multi-functional applications, *Int. J. Extreme Manuf.* 2(3) (2020) 032002. <https://doi.org/10.1088/2631-7990/ab95f6>
- [35] Y. Liu, W. Xiong, D.W. Li, Y. Lu, X. Huang, H. Liu, L.S. Fan, L. Jiang, J.-F. Silvain, Y.F. Lu, Precise assembly and joining of silver nanowires in three dimensions for highly conductive composite structures, *Int. J. Extreme Manuf.* 1(2) (2019) 025001. <https://doi.org/10.1088/2631-7990/ab17f7>

- [36] L. L. Taylor, J. Xu, M. Pomerantz, T. R. Smith, J. C. Lambropoulos, J. Qiao, Femtosecond laser polishing of germanium, *Opt. Mater. Express* 9 (2019) 4165-4177. <https://doi.org/10.1364/OME.9.004165>
- [37] Y. Yang, R. Lou, X. Chen, W. Fan, J. Bai, W. Cao, G. Cheng, J. Si, Influence of energy fluence and overlapping rate of femtosecond laser on surface roughness of Ti-6Al-4V, *Opt. Eng.* 58 (2019) 106107. <https://doi.org/10.1117/1.OE.58.10.106107>
- [38] C. S. Chang, C. K. Chung, J. F. Lin, Surface polishes of the SKD 61 tool steel by a femto pulse laser operating in a wide range of powers, *J. Mater. Process. Technol.* 277 (2020) 116465. <https://doi.org/10.1016/j.jmatprotec.2019.116465>
- [39] S. Gräf, F.A. Müller, Polarisation-dependent generation of fs-laser induced periodic surface structures, *Appl. Surf. Sci.* 331 (2015) 150-155. <https://doi.org/10.1016/j.apsusc.2015.01.056>
- [40] M. Huang, F. Zhao, Y. Cheng, N. Xu, Z. Xu, Origin of laser-induced near-subwavelength ripples: interference between surface plasmons and incident laser, *ACS Nano* 3(12) (2009) 4062-4070. <https://doi.org/10.1021/nn900654v>
- [41] J. Bonse, J. Krüger, S. Höhm, A. Rosenfeld, Femtosecond laser-induced periodic surface structures, *J. Laser Appl.* 24 (2012) 042006. <https://doi.org/10.2351/1.4712658>
- [42] J. Bonse, S. Höhm, S.V. Kirner, A. Rosenfeld, J. Krüger, Laser-induced periodic surface structures— a scientific evergreen, *IEEE J. Sel. Top. Quantum Electron.* 23(3) (2017) 9000615. <https://doi.org/10.1109/jstqe.2016.2614183>
- [43] A. M. Hafiz, E. V. Bordatchev, R. O. Tutunea-Fatan, Experimental analysis of applicability of a picosecond laser for micro-polishing of micromilled Inconel 718 superalloy, *Int. J. Adv. Manuf. Technol.* 70 (2014) 1963-1978. <https://doi.org/10.1007/s00170-013-5408-9>

- [44] Y. D. Chen, W. J. Tsai, S. H. Liu, J. B. Horng, Picosecond laser pulse polishing of ASP23 steel, *Opt Laser Technol* 107 (2018) 180-185. <https://doi.org/10.1016/j.optlastec.2018.05.025>
- [45] M. Osbild, A. Brenner, L. Röther, J. Finger, Ultrashort pulse laser micro polishing of steel – Investigation of the melt pool depth, *Procedia CIRP* 94 (2020) 936-941. <https://doi.org/10.1016/j.procir.2020.09.094>
- [46] A. Sassmannshausen, A. Brenner, J. Finger, Ultrashort pulse laser polishing by continuous surface melting, *J. Mater. Process. Technol.* 293 (2021) 117058. <https://doi.org/10.1016/j.jmatprotec.2021.117058>
- [47] A. Y. Vorobyev, C. Guo, Direct femtosecond laser surface nano/microstructuring and its applications, *Laser Photon. Rev.* 7 (2013) 385-407. <https://doi.org/10.1002/lpor.201200017>
- [48] E. Stratakis, J. Bonse, J. Heitz, J. Siegel, G.D. Tsibidis, E. Skoulas, A. Papadopoulos, A. Mimidis, A.-C. Joel, P. Comanns, J. Krüger, C. Florian, Y. Fuentes-Edfuf, J. Solis, W. Baumgartner, Laser engineering of biomimetic surfaces, *Mater. Sci. Eng. R* 141 (2020) 100562. <https://doi.org/10.1016/j.mser.2020.100562>